Cent. Eur. J. Geosci. • 6(3) • 2014 • 257-278
DOI: 10.2478/s13533-012-0188-6

VERSITA

Central European Journal of **Geosciences**

Dispersion modeling of air pollutants in the atmosphere: a review

Research Article

Ádám Leelőssy[1], Ferenc Molnár Jr.[2], Ferenc Izsák[3], Ágnes Havasi[3], István Lagzi[4], Róbert Mészáros[1]*

1 *Department of Meteorology, Eötvös Loránd University, Budapest, Hungary*

2 *Department of Physics, Applied Physics, and Astronomy, Rensselaer Polytechnic Institute, Troy, New York, USA*

3 *Department of Applied Analysis and Computational Mathematics, Eötvös Loránd University, Budapest, Hungary*

4 *Department of Physics, Budapest University of Technology and Economics, Budapest, Hungary*

Received 22 October 2013; accepted 15 May 2014

Abstract: Modeling of dispersion of air pollutants in the atmosphere is one of the most important and challenging scientific problems. There are several natural and anthropogenic events where passive or chemically active compounds are emitted into the atmosphere. The effect of these chemical species can have serious impacts on our environment and human health. Modeling the dispersion of air pollutants can predict this effect. Therefore, development of various model strategies is a key element for the governmental and scientific communities. We provide here a brief review on the mathematical modeling of the dispersion of air pollutants in the atmosphere. We discuss the advantages and drawbacks of several model tools and strategies, namely Gaussian, Lagrangian, Eulerian and CFD models. We especially focus on several recent advances in this multidisciplinary research field, like parallel computing using graphical processing units, or adaptive mesh refinement.

Keywords: air pollution modeling • Lagrangian model • Eulerian model • CFD; accidental release • parallel computing

1. Introduction

Chemical species including toxic materials have various emission pathways into the atmosphere. They can be emitted either from approximately point sources (e.g., accidental release at nuclear power plants (NPP) or volcanic eruptions) or from area sources (e.g., emission of photochemical smog precursors and forest fires). Moreover, time interval of releases can be diversified. These air pollutants can travel hundreds, even thousands of kilometres from their release across the globe depending on their chemical and physical properties (e.g., chemical composition, solubility in water, or size distribution for aerosol particles), and they affect the human health and result in a long-term effect on our environment. Such incidents can have a huge economic impact. For example the eruption of Eyjafjallajökull in Iceland over a period of six days in April, 2010 caused enormous disruption to air travel in most parts of Europe because of the closure of airspace, due to volcanic ash ejected to the atmosphere. The estimated loss of airlines' revenue was about US$ 1.7 billion [1]. Another emblematic example is the effect of the photochemical air pollution. Photochemical smog can affect human health and reduce crop yield due to its oxidative nature. To save

*E-mail: mrobi@nimbus.elte.hu

human lives and to reduce economic losses, computational models of air pollutant dispersion are being developed to understand and predict the outcome of these phenomena and accidents.

Model simulations should be fast and must have a high degree of accuracy to be used in real time applications (e.g., decision support). Therefore, one of the main challenge of atmospheric dispersion modeling is to develop models and software that can provide numerical predictions in an accurate and computationally efficient way. Disaster at Chernobyl NPP has stimulated the development of such accidental release and decision support software (e.g., RODOS). Underestimating the concentrations or doses of air pollutants (e.g., radionuclides) can have serious health consequences. However, in case of overestimation in regions where significant dose will not be reached would waste valuable human and financial resources.

The transport and transformation of air pollutants in the atmosphere is mainly governed by advection (wind field). Other processes such as turbulence, chemical reactions, radioactive decay and deposition can also play important roles in the dispersion of toxic substances. Therefore, strategies for model development require an interaction of researchers from different fields (e.g., meteorology, geophysics, chemistry, IT).

Another important issue in modeling the dispersion of air pollutants is the analysis of the lifetime of the chemical species and the characteristic distance that species can be transported, which is correlated with the lifetime. If the emitted species have short lifetime (minutes-hours) in the atmosphere (usually reactive species or aerosols), they cannot be transported long-range and their effects will be concentrated on local scale (e.g., effect of the PM – particulate matter). However, chemical species such as NO_x, SO_2, which have longer lifetimes (hours-days) can have wider impact zones. Therefore, in such cases regional or continental modeling approaches are needed. Some pollutants (e.g., CO, NH_3) have long lifetimes (days-weeks) resulting in long-range transport, so for these pollutants continental and global transport models need to be employed.

For simulating the dispersion of air pollutants, various modeling approaches have been developed. The main aim of this article is to provide a brief review of air pollution modeling tools and their application. The paper is structured as follows. Section 2 provides a general overview of the related physical problems and air pollution modeling. The following three sections describe three families of models: Gaussian, Lagrangian and Eulerian dispersion models in detail with their advantages and drawbacks. Finally, Sections 6 and 7 discuss parallel computing and computational fluid dynamics models for environmental modeling.

2. Overview of atmospheric dispersion modeling

In this section we will give a brief overview how to describe mathematically and parameterize various important processes in the atmosphere. We will start with the atmospheric transport equation, which describes the spatial-temporal change of the concentrations of air pollutants. Next we will focus on turbulent parameterization and finally show how to handle deposition and chemical transformation in the atmosphere.

2.1. The transport equation

In a fluid, the mass conservation of a component described by concentration c can be expressed as:

$$\frac{\partial c}{\partial t} = -\nabla\cdot(c\vec{v}) + S_c + \nabla\cdot(D_c\nabla c). \tag{1}$$

where $\vec{v}$ is the wind vector, S_c is the source term and D_c is the diffusion coefficient. Eq. (1) represents the change of the concentration at a specified point as the sum of the advective flux, the source terms and the diffusive flux, respectively. Dry and wet deposition and chemical or radioactive decay are part of the S_c term, while gravitational settling can be added as an extra advection component. Turbulent diffusion, however, is not represented in Eq. (1). Turbulence is usually taken into account with Reynolds' theory that splits the wind and concentration field into time-averaged and turbulent perturbation values:

$$\vec{v} = \bar{\vec{v}} + \vec{v}' \tag{2}$$

$$c = \bar{c} + c' \tag{3}$$

For turbulent flows, the transport equation can be written in the same form as Eq. (1) with the addition of three eddy covariance terms, yielding a form that is widely used in atmospheric dispersion modeling:

$$\begin{aligned}\frac{\partial \bar{c}}{\partial t} = &-\nabla\cdot(\bar{\vec{v}}\bar{c}) + S_c + D_c\nabla^2\bar{c} - \frac{\partial\overline{(u'c')}}{\partial x} \\ &- \frac{\partial\overline{(v'c')}}{\partial y} - \frac{\partial\overline{(w'c')}}{\partial z}\end{aligned} \tag{4}$$

The right hand side of Eq. (4) describes advection, source terms, molecular diffusion and horizontal and vertical turbulent fluxes. In the atmosphere, turbulent mixing is several orders of magnitude more efficient than molecular diffusion, thus the third component of Eq. (4) can usually be neglected, except in the laminar ground layer.

To calculate the eddy covariance terms in Eq. (4), the gradient transport theory was developed as an analogy of Fick's law for molecular diffusion. Gradient transport theory is based on the assumption that the turbulent flux is proportional to the gradient of the concentration field. This approach leads to a form where turbulent fluxes are expressed as an additional diffusion term:

$$\frac{\partial \bar{c}}{\partial t} = -\nabla\cdot(\bar{\vec{v}}\bar{c}) + S_c + D_c\nabla^2\bar{c} + \nabla\cdot(\underline{\underline{K}}\nabla\bar{c}), \qquad (5)$$

where $\underline{\underline{K}}$ is a diagonal matrix of the eddy diffusivities K_x, K_y, K_z. Due to the different atmospheric turbulent processes in horizontal and vertical directions, $\underline{\underline{K}}$ cannot be assumed to be isotropic. Furthermore, while D_c is a property of the chemical species, $\underline{\underline{K}}$ is a property of the flow, thus it varies in both space and time. Assuming an incompressible fluid, isotropic horizontal turbulence and neglecting the molecular diffusion, the transport equation can be written in the form:

$$\frac{\partial \bar{c}}{\partial t} = -\bar{\vec{v}}\nabla\bar{c} + S_c + \nabla_h\cdot(K_h\nabla_h\bar{c}) + \frac{\partial}{\partial}K_z\frac{\partial\bar{c}}{\partial z}, \qquad (6)$$

where ∇_h is the horizontal divergence operator, K_h is the horizontal and K_z is the vertical eddy diffusivity. The eddy diffusivities describe the turbulence intensity in the boundary layer, considering both thermal and kinetic turbulence. The vertical profile of eddy diffusivities is calculated through various parameterizations based on methods briefly described in Chapter 2.2.

2.2. Turbulence parameterization

Near-surface atmospheric turbulence is caused by mechanical and thermal effects. Friction forces in a viscous flow generate mechanical turbulence, which is driven by wind shear. Therefore, three-dimensional wind field data is necessary to estimate the intensity of mechanical turbulence. However, near-surface wind shear can be estimated using the surface roughness, a parameter that represents the strength of friction between the surface and the atmosphere.

Thermal turbulence is driven by buoyancy and can be characterized with atmospheric stability measures. Surface radiation budget has a critical effect on atmospheric stability, therefore correct estimation of sensible and latent heat fluxes has a key importance in the estimation of thermal turbulence intensity. Under stable conditions, the boundary layer turbulence is dominated by mechanical effects, thus turbulent mixing is driven by wind shear (stable boundary layer, SBL). In unstable atmosphere, turbulence is mostly generated by thermal convection (convective boundary layer, CBL).

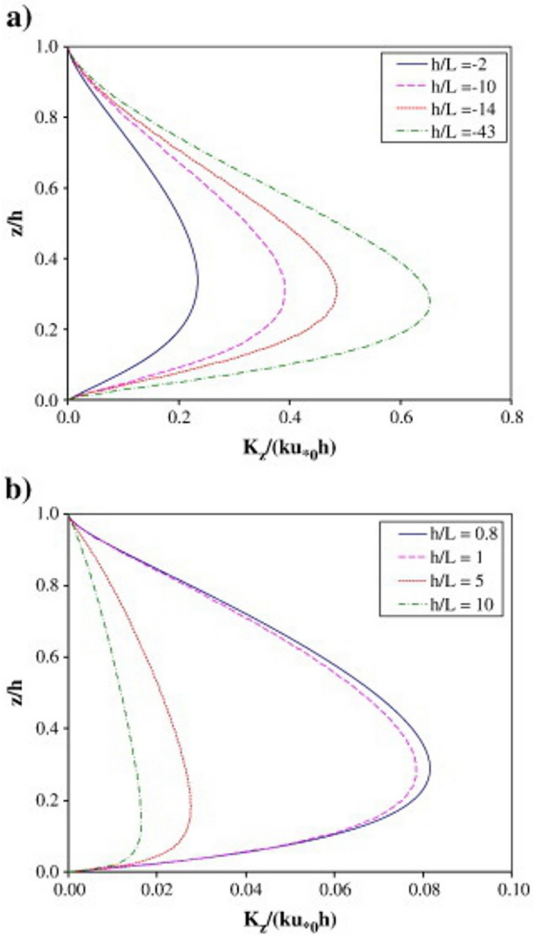

Figure 1. Profiles of the normalized vertical eddy diffusivity for different normalized planetary boundary layer heights under (a) unstable conditions and (b) stable conditions from [3], where h is the planetary boundary layer height and L is the Monin–Obukhov length, respectively (see section 2.2.3).

Turbulence intensity can be described using various measures. Using the standard Reynolds-averaged (RANS) approach of turbulence, the turbulent kinetic energy (TKE, J kg^{-1}) represents the average kinetic energy of the subgrid scale wind fluctuations [2]:

$$TKE = \frac{1}{2}\left(\overline{u'^2} + \overline{v'^2} + \overline{w'^2}\right), \qquad (7)$$

where u', v', w' are wind component fluctuations with respect to the time-averaged wind.

Dispersion-oriented turbulence characteristics try to estimate the mixing efficiency instead of describing the turbulence itself. Mixing efficiency is often treated as the deviation of a Gaussian plume, which is widely used in Gaussian (section 3) and puff (section 4.2) models.

The vertical profile of vertical eddy diffusivity (Figure 1) shows near-zero values very close and very far from ground,

Table 1. Pasquill's stability classes: very unstable (A), unstable (B), slightly unstable (C), neutral (D), slightly stable (E) and stable (F) boundary layer. Note: neutral (D) class has to be used for overcast conditions and within one hour after sunrise / before sunset [7].

	Daytime insolation			Night time	
Surface wind speed	Strong	Moderate	Slight	Thin overcast or max. 3 octas low cloud	Min. 4 octas low cloud
< 1 m/s	A	A	B	E	F
1 – 3 m/s	A	B	C	E	F
3 – 5 m/s	B	C	C	D	E
5 – 8 m/s	C	D	D	D	D
> 8 m/s	D	D	D	D	D

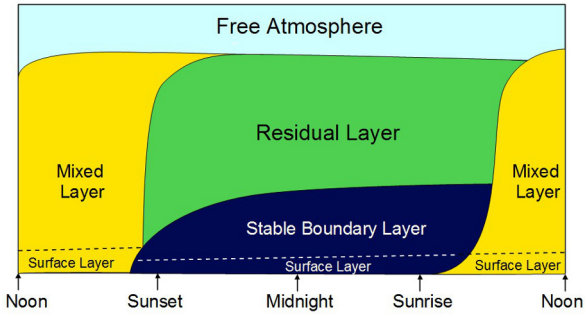

Figure 2. A typical daily cycle of the planetary boundary layer in fair weather (after [2]).

and a maximum in the lower part of the boundary layer [3]. In the region above the maximum diffusivity, the height where vertical turbulent mixing becomes negligible is defined as h planetary boundary layer (PBL) height. Negligible vertical turbulence causes no upward transport of air pollutants, thus pollution of sources in the PBL will remain in the boundary layer. Concentration values are largely influenced by the volume that is available for the dilution of released pollutants in a given period of time; this volume is defined by the PBL height and the advection velocity.

Intensity of boundary layer turbulence has a significant diurnal and annual variability [4]: PBL height can reach 2000 m or above in convective situations, typically in the summer, but can be as low as 10–50 meters on clear nights with low wind speed. The daytime mixed layer collapses shortly before sunset, when direction of surface heat fluxes is reversed and thermal turbulence is ceased (Figure 2). Thermal turbulence driven boundary layers are often referred to as convective boundary layer (CBL), while in stable boundary layers (SBL), stable thermal stratification destroys mechanical turbulence. An SBL keeps pollutants from surface sources close to the ground causing significantly higher concentrations than a CBL, especially during nighttime.

2.2.1. Stability classes

Turbulent mixing in the atmosphere is driven by wind shear and buoyancy. An obvious approach to calculate turbulence parameters is to define categories regarding radiation parameters, wind speed, surface roughness and cloud cover. The widely used method of Pasquill defines six stability classes from the very unstable A to the moderately stable F based on wind speed, sun elevation and cloud cover (Table 1) [5, 6]. The advantage of Pasquill's method is that turbulence parameters can be directly estimated from basic meteorological measurements; however, the accuracy of pre-defined values of the six discrete classes is often low compared to more sophisticated parameterizations.

2.2.2. Richardson number

The ratio of the thermal to mechanical turbulence is characterized by the gradient Richardson number [8]:

$$R_i = \frac{-\frac{g}{\rho_0}\frac{\partial \rho}{\partial z}}{\left(\frac{\partial u}{\partial z}\right)^2 + \left(\frac{\partial v}{\partial z}\right)^2}, \tag{8}$$

where ρ_0 is the reference density and g is the surface acceleration of gravity. Thermal turbulence (buoyancy) is described by the numerator of Eq. (8), while a wind shear term is present in the denominator. While buoyancy can have both positive and negative impact on turbulence intensity depending on the direction of the density gradient, the positive wind shear term is always a generator of turbulence.

Negative Richardson number values indicate unstable stratification that develops thermal turbulence, while small positive Richardson numbers correspond to stably stratified atmosphere with significant wind shear and mechanical turbulence. At large positive Richardson numbers, thermal stability destroys mechanical turbulence and results in a stable boundary layer. Typical values of Richardson number are given in Table 2.

Table 2. Typical values of the Richardson number and the Monin–Obukhov-length at each stability class [15].

Stability class	Richardson number	Monin–Obukhov-length (m)
A	$R_i < -0.86$	–2 to –3
B	$-0.86 \leq R_i < -0.37$	–4 to –5
C	$-0.37 \leq R_i < -0.10$	–12 to –15
D	$-0.10 \leq R_i < 0.053$	Infinite
E	$0.053 \leq R_i < 0.134$	35 to 75
F	$0.134 \leq R_i$	8 to 35

2.2.3. Monin–Obukhov theory

The most widely used approach to describe vertical profile of turbulence intensity was developed by Monin and Obukhov in 1954. They combined the turbulent vertical fluxes of heat and momentum into a parameter with dimension of length, the L Monin–Obukhov-length:

$$L = -\frac{\left(-\overline{u'w'}\right)^{\frac{3}{2}}}{\kappa \frac{g}{T}\overline{T'w'}}, \tag{9}$$

where T', u', w' are the temperature, horizontal and vertical wind turbulent fluctuations, T is the temperature and κ is the von Kármán constant, usually taken equal to 0.4 [2]. Hardly measurable turbulent fluxes can be estimated with the definition of two parameters: the friction velocity u^* and the turbulent heat flux q. There are different methods for the determination of u^* and q using net radiation components and (potential) temperature gradient, which largely differ in the convective and in the stable boundary layer [9, 10].

The Monin–Obukhov length in Eq. (9) is a reference scale for boundary layer turbulence, thus any height z can be given with the dimensionless stability parameter z/L. Monin and Obukhov defined universal functions for neutral, stable and unstable cases that describe the vertical profiles of wind and temperature as a function of the z/L height [11]. The eddy diffusivities in Eq. (6) are parameterized based on the vertical profiles obtained from the Monin–Obukhov-theory (Figure 1) [3].

The Monin–Obukhov theory was validated against numerous measurement and advanced computational fluid dynamics datasets, and although some weaknesses were shown, it still provides the most reliable basis for all fields of atmospheric modeling [3, 9, 10, 12–14]. Typical values of the Monin–Obukhov-length are given in Table 2.

2.3. Deposition

The removal of gases and particulates from the atmosphere can occur by dry or wet deposition (Figure 3). The importance of each deposition form varies with species and locations. Dry deposition is a continuous process, while wet removal can be realized only in the presence of precipitation. Both dry and wet depositions depend on the properties of the gases or particles, and removal processes are governed by several environmental factors. The effect of both dry and wet depositions can be incorporated in models as a first order reaction taking into account dry deposition (k_d) and wet deposition (k_w) coefficients through reaction $\frac{dc_i}{dt} = -k_{w/d}c_i$, where c_i is the concentration of the i component of the system.

2.3.1. Dry deposition

The exchange of trace gases between the surface and the atmosphere is mainly governed by turbulent diffusion. The deposition can be estimated by the widely used „big-leaf" model, in which the deposition velocity is defined as the inverse of the sum of the atmospheric and surface resistances [16–18]:

$$v_d = (R_a + R_b + R_c)^{-1}, \tag{10}$$

where R_a, R_b, and R_c are the aerodynamic resistance, the quasi-laminar boundary layer resistance, and the canopy resistance, respectively. Each term is given by more or less detailed parameterization in different models. The deposition of numerous trace gases (e.g., ozone, nitrogen oxides, ammonia) can be estimated using this simple model. In contrast to the previous case, the dry deposition of particles is highly dependent on their characteristic size. Smaller particles are deposited similarly as gases, while the removal of larger ones is mainly governed by gravitational settling (sedimentation). Dry deposition processes for particles with a size between 0.1 and 1 μm are less efficient. The dry deposition velocity can be written then as [19]:

$$v_d = v_g + \frac{1}{R_a + R_b + v_g R_a R_b}, \tag{11}$$

where v_g is the gravitational settling velocity (or terminal settling velocity), and the resistance terms R_a, and R_b are the same as those for gases (see above). As we assume that all deposited particles stick to the surface, the surface resistance (R_c) is zero for particles.

The dry deposition coefficient, k_d, can be derived from the deposition or settling velocity simply dividing it by a characteristic height, where the deposition occurs.

2.3.2. Wet deposition

Precipitation cleanses the air by capturing pollutants and depositing them onto the surface. The efficiency of this process can be expressed by the fractional depletion rate of pollutant concentrations in the air. This rate is generally characterized by the so-called scavenging coefficient.

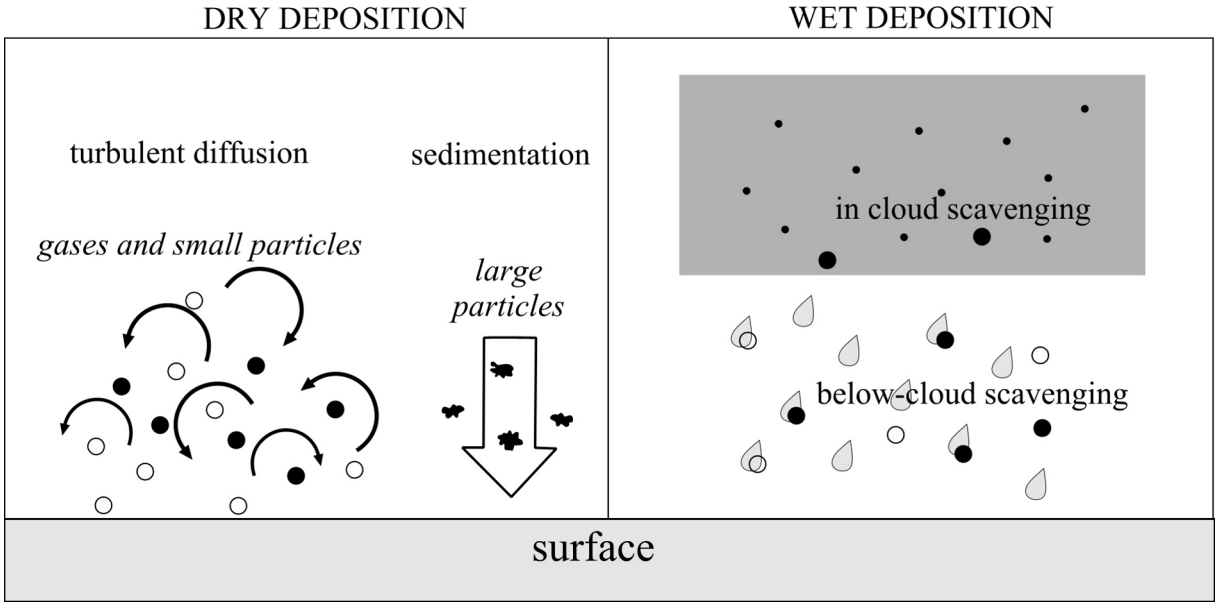

Figure 3. Dry and wet deposition processes in the atmosphere.

During the parameterization of wet deposition (or wet scavenging), in-cloud scavenging (rainout) and below-cloud scavenging (washout) are usually distinguished. However, for a more complete estimation of wet deposition, explicit information about clouds and precipitation rate at all model levels would be required. Instead of these complex parameterization schemes [19], the wet deposition is often estimated by a simple method in chemical transport models. The species dependent scavenging coefficient (kw in s^{-1}) can take the simple form:

$$k_w = AP^B, \tag{12}$$

where P is the rate of rainfall (in mm h^{-1}) and A and B are constants specific for gas or aerosol particle. In some models A and B vary also as a function of scavenging type (rainout, washout), or in case of aerosol particles as a function of particle radius [20].

2.4. Chemical reactions and radioactive decay

Chemical reactions and transformations (e.g., radioactive decay) of air pollutants can be very complex in the atmosphere, where thermal and photochemical reactions can simultaneously occur. Photochemical reactions usually produce radicals that have high affinity to react with each other and with other chemical species in the atmosphere. These radicals can initiate various reactions, and reactions in the atmosphere can be described as a complex reaction network. This reaction network can be interpreted as a set of reaction mechanisms. A reaction mechanism consists of elementary reactions by which overall chemical change occurs. Chemical reactions can be described and calculated by a set of ordinary differential equations (ODEs)

$$\frac{dc_i}{dt} = \sum_n k_n \prod_i c_i^{\alpha_n^i}, \tag{13}$$

where k_n is the chemical rate coefficient for the n^{th} reaction and α_n^i is the order of reaction with respect to chemical species i.

Radioactive decay differs from chemical reactions due to its nature, because during the radioactive decay the atomic properties are changed. However, from the mathematical point of view this process can be interpreted as a first order chemical reaction:

$$\frac{dc_i}{dt} = -kc_i, \tag{14}$$

The solution of Eq. (14) is a monotonically decreasing exponential function with time. The radioactive decay constant k is an inherent property of the radionuclides. In models, consecutive decays can be easily taken into account and the solution can be expressed analytically. In environmental models Eqs. (13)–(14) are included in the source term (S_c) of the atmospheric transport equation [Eq. (10)]. Eulerian models can easily handle this mean field description by using (quasi-continuous) concentration field.

However, if the dispersion of chemical species are considered as a transport of small particles (e.g., in Lagrangian models), application of the chemical and decay rate constants are meaningless, because these quantities represent "bulk" properties of the system, and they are not related to property of individual particles. This problem can be overcome using a probabilistic description of the processes (radioactive decay, first order chemical reaction and deposition). The probability that individual particles during a time step will transform, decay or deposit can be calculated by the following expression

$$p = 1 - e^{-k\Delta t}, \tag{15}$$

where k is either the "macroscopic" first order rate constant (reaction rate constant, radioactive decay constant) or wet/dry deposition constant. In this way microscopic quantities can be coupled to macroscopic properties.

3. Gaussian dispersion models

3.1. Theory and limitations of Gaussian models

The transport equation [Eq. (6)] is a partial differential equation that can be solved with various numerical methods described in section 5. Assuming a homogeneous, steady-state flow and a steady-state point source at $(0, 0, h)$, Eq. (6) can also be analytically integrated and results in the well-known Gaussian plume distribution (see derivation in [21]):

$$\bar{c}(x, y, z) = \frac{Q}{2\pi\sigma_y\sigma_z\bar{u}} \exp\left(\frac{-y^2}{2\sigma_y^2}\right)\left(\exp\left(\frac{-(z-h)^2}{2\sigma_z^2}\right) + \exp\left(\frac{-(z+h)^2}{2\sigma_z^2}\right)\right), \tag{16}$$

where $\bar{c}$ is the time-averaged concentration at a given position, Q is the source term, x is the downwind, y is the crosswind and z is the vertical direction and $\bar{u}$ is the time-averaged wind speed at the height of the release h. The standard deviations σ_y and σ_z describe the crosswind and vertical mixing of the pollutant. Eq. (16) describes a mixing process that results in a Gaussian concentration distribution both in crosswind and in vertical directions, centered at the line downwind from the source (Figure 4). The last term of Eq. (16) expresses a total reflection from the ground.

Gaussian models have an extremely fast response time, because they only calculate a single formula (Eq. (16) or similar) for each receptor point instead of solving differential equations. This calculation is almost immediate even on common computers, however, meteorological data preprocessing and sophisticated turbulence parameterizations can increase the computational cost. Gaussian models are widely applied in decision support software where robust model setup and fast response time is a key priority [22].

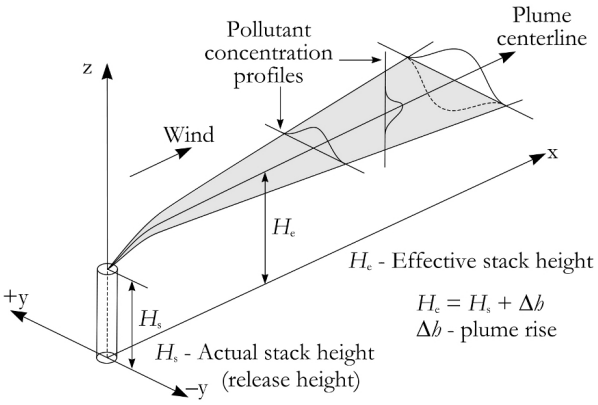

Figure 4. Schematic figure of a Gaussian plume. The effective stack height H_e and the crosswind and vertical deviation of the profile are the key parameters of the model.

Gaussian models provide poor results in situations with low wind speeds, where the three-dimensional diffusion is significant. Unfortunately, these situations have proven to be the most dangerous ones in real-life atmospheric dispersion problems as they are often connected to a stably stratified atmosphere or low-level inversions [23]. Inspired by the fast increasing computational capacity and serious environmental incidents, Gaussian models have been developed to increase their accuracy and take into account some of the unrepresented physical processes. In state-of-the-art Gaussian models like AERMOD, CTDM or ADMS, the impact of complex terrain [10] or convective boundary layer turbulence [24] is parameterized to provide more accurate prediction in environmental applications.

One of the most widely used atmospheric dispersion model is the open-source AERMOD, developed by the US Environmental Protection Agency (EPA). AERMOD includes modules to handle complex terrain and urban boundary layer [9], as well as the Plume Rise Model Enhancements (PRIME) algorithm to estimate downwash effects near buildings. AERMOD calculates eddy diffusivities based on the Monin–Obukhov-theory (see section 2.2.3).

Despite the advanced features of AERMOD, it still uses a steady-state approximation for the flow and the source, thus it can be used only within a distance of 10–100 km from the source. It is mostly used for long-term statistical impact studies to estimate air pollution around industrial

sites [26, 27], environmental protection or agricultural areas [28, 29]. For mountain regions, EPA has also developed the Complex Terrain Dispersion Model (CTDM) that provides tools to estimate concentrations above complex terrain without the costly simulation of the mesoscale wind field [10].

Besides AERMOD, the British ADMS model is also widely used for air quality simulations. It provides a range of modules specified for different locations like urban, coastal or mountain areas, and is able to calculate deposition and radioactive doses [30]. ADMS has become very popular in Europe for environmental impact studies and urban air quality prediction [31]. For the latter purpose, ADMS-Urban module includes pre-defined emission scenarios and a chemistry model to calculate interactions between plumes of several point and line sources in an urban area [32].

There are several other Gaussian models available like CALINE3 for highway air pollution, OCD for coastal areas, BLP and ISC for industrial sites or ALOHA for accidental and heavy gas releases (see [33] for a detailed list). They are widely used by authorities, environmental protection organizations and industry for impact studies and health risk investigations [34, 35]. Their short runtime allows the users to make long-term statistical simulations [36, 37] or detailed sensitivity studies [5, 38], and provide immediate first-guess information in case of an accidental release. They are often coupled with GIS software to create an efficient decision support tool for risk management [22, 39].

While the earlier industrial incidents in Seveso (Italy) and Bhopal (India) and other air pollution episodes had been concentrated on a local scale, the Chernobyl accident in 1986 had serious consequences in several countries and the radioactive 131I gas was measured globally [40]. It was clear that the steady-state assumption of Gaussian models could not handle continental scale dispersion processes, however, existing Eulerian and Lagrangian models provided precious information in the estimation of the impact of the accident [40, 41]. The fast development of computers and NWP (Numerical Weather Prediction) models allowed researchers to create more and more efficient dispersion simulations using gridded meteorological data. Eulerian and Lagrangian models, presented in sections 4 and 5, are state-of-the-art tools of recent atmospheric dispersion simulations [42–44].

4. Lagrangian models

Lagrangian models calculate trajectories of air pollutants driven by deterministic (wind field and buoyancy) and stochastic (turbulence) effects.

These trajectories are calculated based on ordinary differential equations (ODEs) instead of using partial differential equations (PDEs) in the original dispersion problem, which is computationally an easy task, and avoids spatial truncation errors and numerical diffusion. The final distribution of a large number of particles gives an estimation of the concentration field.

Computational cost of Lagrangian models is independent of the output grid resolution, therefore this approach is exceptionally efficient for short-range simulations compared to gridded computations with very fine resolution. However, long-range simulations require the calculation of a large number of single trajectories that rapidly increases the computational cost. Nested models use Lagrangian approach near the source and interpolate the concentration field to an Eulerian grid at a given distance to perform large-scale Eulerian simulation [45, 46].

The trajectory equation for a single particle is an ordinary differential equation

$$\frac{d\vec{r}}{dt} = \vec{v} + \vec{v}_1, \tag{17}$$

where $\vec{r}$ is the position of the particle, $\vec{v}$ is the deterministic particle speed (consisting of advection, settling and buoyancy), while $\vec{v}_1$ is the turbulent wind fluctuation vector. The turbulent fluctuation is often estimated as a random walk, described by the Langevin equation [47]:

$$dw_t = -\frac{W_t}{T_L}dt + \sqrt{\frac{2\sigma_w^2}{T_L}}dW. \tag{18}$$

Where w_t is the vertical turbulent fluctuation, T_L is a Lagrangian integration time step, σ_w is the vertical turbulent velocity fluctuation and dW represents a white noise process with mean zero and variance d_t. The Lagrangian timescale T_L is a key parameter and is often given explicitly [48], or computed from velocity fluctuations [14]. Numerical representation of the white noise process in Eq. (18) requires an efficient random number generator that can significantly increase the computational cost of the model.

4.1. Puff models

Puff models show similarities with both Gaussian and Lagrangian dispersion models. They treat the pollution as a superposition of several clouds, "puffs" with a given volume, and calculate the trajectories of these puffs. Puff models separate the model physics by scale: the sub-puff scale processes are treated with Gaussian approach (Eq. (16) or similar), while above the puff size, Lagrangian trajectories are calculated [48]. The result is a Gaussian plume transported along a wind-driven trajectory instead of a straight centerline as in the standard Gaussian approach (Figure 5). The final concentration field is given as a

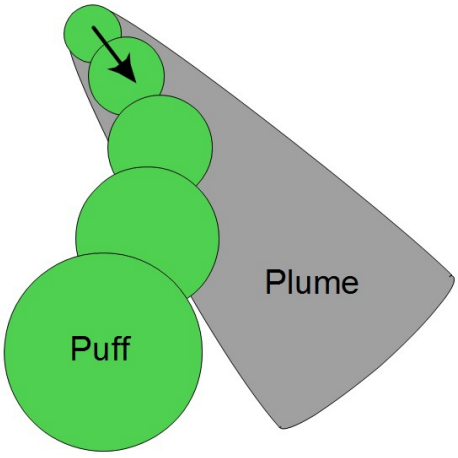

Figure 5. Schematic representation of Gaussian plume and puff models. Puff models still estimate a Gaussian dispersion, but are able to take into account temporal and spatial wind changes.

superposition of the concentration field of each puff. With this two-way approach, puff models can handle spatial and temporal changes of wind direction with keeping the computational cost reasonably low.

Puff models include the effect of turbulence in two different ways: with a stochastic random-walk approach in the trajectories of the puffs (Eqs. (17)-(18)); and through the deviation of a normal distribution inside each puff. It can be interpreted as a separated treatment of large-scale and sub-puff-scale turbulence.

Several puff models are available with a wide range of applications in risk management and environmental protection [45, 49, 50]. The Danish RIMPUFF model is part of the RODOS decision support system, the European framework for nuclear security [51]. The US EPA offers the CALPUFF system as a preferred model for environmental protection and public health studies. CALPUFF has been used worldwide for scientific and regulatory purposes [52–55]. The RAPTAD puff model was specifically designed for simulations around complex terrain [56, 57] with both industrial and urban applications [58, 59].

One of the most popular dispersion models is HYSPLIT, a hybrid puff-particle model developed by the NOAA Air Resources Laboratory. HYSPLIT has been used in numerous studies to estimate consequences of an accidental release or identify source regions of pollution [60–63]. It can be run in both single trajectory and puff mode, or with a mixture of a vertical trajectory and a horizontal puff simulation [64, 65].

4.2. Trajectory models

Trajectory models perform stochastic simulation of numerous single point particles, each of them corresponding to a fraction of the released mass of pollution. The trajectory of a single particle is driven by advection, buoyancy and turbulence (random walk), calculated through Eqs. (17)–(18). Trajectory models provide a fine estimation of turbulent mixing without solving partial differential equations, on the other hand, a large number of single trajectories have to be calculated that largely increases the computational cost.

With the fast increase of computational capacity, trajectory models have become state-of-the-art tools of regional to global scale atmospheric dispersion simulations with calculation of millions of long-range trajectories [42, 66]. Two of the most popular models are the NAME, developed by the UK Met Office, and the open-source FLEXPART. NAME and FLEXPART have an impressive background of validation studies and environmental applications [66–69] and provided valuable information for authorities in critical situations like the 2001 foot-and-mouth disease epidemic [49], the Eyjafjallajökull eruption [42] or the Fukushima nuclear accident [44, 70]. We note that the HYSPLIT model, presented in section 4.1 as a hybrid puff-trajectory model, can also be used in trajectory mode.

Besides the prediction of air quality and dispersion pathways, trajectory models are often used in backward mode to identify source regions of air pollution [63, 71, 72].

Backward simulations provide a source-receptor sensitivity field that corresponds to probabilities of possible source locations [71].

5. Eulerian models for solving atmospheric transport equation

5.1. General principles

The main idea in the Eulerian models is to solve numerically the atmospheric transport equation [Eq. (1)] in a fixed coordinate frame. Mathematically, it is a second order partial differential equation, and its solution with the appropriate initial and boundary conditions provides the spatiotemporal evolution of the concentration . There are several numerical methods to solve PDEs. In general, these methods consist of two steps: (i) spatial discretization, (ii) the temporal integration of the derived ordinary differential equations. The spatial discretization, which is mostly performed on a grid, reduces the PDE to a system of ODEs depending on a single (time) variable. The system of ODEs then can be solved as an initial value problem,

Table 3. Principles in the time integration.

	explicit	implicit
One-step	$\{c_{i,j}^n\} \to \{c_{i,j}^{n+1}\}$	$\{c_{i,j}^n, c_{i,j}^{n+1}\} \to \{c_{i,j}^{n+1}\}$
Multistep	$\{c_{i,j}^{n-k}, \ldots, c_{i,j}^n\} \to \{c_{i,j}^{n+1}\}$	$\{c_{i,j}^{n-k}, \ldots, c_{i,j}^{n+1}\} \to \{c_{i,j}^{n+1}\}$

and a variety of powerful methods and software tools exist for this purpose.

There are several Eulerian models developed and used by a large number of scientific communities. The GEOS–Chem model is a global three-dimensional dispersion model using assimilated meteorological observations from the Goddard Earth Observing System of the NASA Global Modeling and Assimilation Office. This model can be used to solve various atmospheric composition problems on global scale [73]. WRF-Chem is the Weather Research and Forecasting (WRF) model coupled with chemical transformations occurring in the atmosphere. The model takes into account the emission, transport, turbulence and reactions of chemical compounds in gas phase and aerosols coupled to the meteorology. The model can be used for investigation of regional-scale air quality problems and cloud-scale interactions between clouds and chemistry [74]. The Community Multi-scale Air Quality (CMAQ) modeling system has been developed to solve multiple air quality issues, such as tropospheric ozone, aerosols and acid deposition. CMAQ is a multi-platform model that can be used for either urban or regional scale air quality modeling. For this purpose governing equations in the model are expressed in a generalized coordinate system. CMAQ simulates various chemical and physical processes that are important in tropospheric trace gas transformations. The model contains three types of modeling components: a meteorological modeling system for the description of atmospheric states and motions, emission models for man-made and natural emissions and a chemistry-transport modeling system for simulation of the chemical reactions [75].

To illustrate the concept of Eulerian models, we will present some techniques for a two-dimensional atmospheric transport equation

$$\frac{\partial c}{\partial t} = -u\frac{\partial c}{\partial x} + K_x\frac{\partial^2 c}{\partial x^2} + K_y\frac{\partial^2 c}{\partial y^2}, \quad u > 0 \qquad (19)$$

on the physical domain Ω. This equation describes a simplified situation, where the spread of a pollutant occurs by advection (wind) and turbulent diffusion. Here we adjust the coordinate system to the direction of the wind, which is assumed to be steady. To have a well-posed problem, we need to complete Eq. (19) with initial and boundary conditions. In the derivations, we use homogeneous Dirichlet boundary conditions, namely, we assume that the concentration is zero at the boundary of the physical domain, which is a good approximation if the boundaries are far away from the source.

5.2. A simple approach: the finite difference method

In this simple approach, all the derivatives are approximated by finite differences. The spatial derivatives are discretized on a grid with uniform rectangles of size $\Delta x \times \Delta y$. We assume that c is sufficiently smooth (differentiable). This is justified by the presence of the diffusion term. We use the notation $c_{i,j}^n$ to approximate the values of $c(n\Delta t, x_i, y_j)$ at the n^{th} time level and at grid points (x_i, y_j). As a feasible choice we can use central finite differences

$$\frac{c_{i+1,j}^n - c_{i-1,j}^n}{2\Delta x} \quad \text{and} \quad K_x\frac{c_{i+1,j}^n - c_{i-1,j}^n}{(\Delta x)^2} \qquad (20)$$

to approximate the derivatives $\frac{\partial}{\partial x}$ and $K_x\frac{\partial^2}{\partial x^2}$, respectively in the grid point (x_i, y_j) on the right hand side of Eq. (20). In both cases, the truncation error is $O(\Delta x)^2$. Additionally, the approximations of the derivatives should be modified such that the boundary condition $c_{i,j}^n$ for all n is incorporated for those indices (i, j) which lie on the boundary. To simulate the time evolution in Eq. (20), we first recognize that the above procedure results in an ODE system, where the unknowns are the values $c_{i,j}^n$ with $n \in \left(0, \frac{T}{\Delta t}\right)$. To approximate it for $n = 1, 2, \ldots$ we should apply time integration, or in other words, we have to use an ODE solver. This can be either explicit or implicit and can contain one or more time steps.

Explicit methods are easy to implement and can be calculated quickly: here using the values $\{c_{i,j}^n\}$ for all possible indices i and j one can calculate the values $\{c_{i,j}^{n+1}\}$. It is also possible that for the calculation of the values $\{c_{i,j}^{n+1}\}$ we already use them, which results in a system of equations to be solved for these unknowns. These possibilities are depicted in Table 3.

As an example, we give a finite difference scheme for Eq. (20), where second order differences are used for the spatial approximation and the time integration is executed using the so-called Crank–Nicolson method:

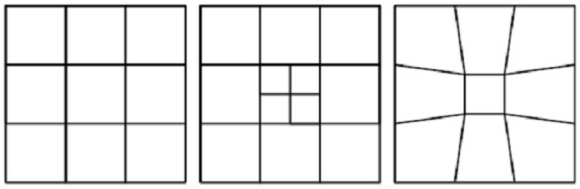

Figure 6. Uniform grid (left) and examples of h-refinement (center) and r-refinement (right). Reprinted with permission from [76].

$$
\begin{aligned}
c_{i,j}^{n+1/2} &= \frac{c_{i,j}^{n} + c_{i,j}^{n+1}}{2} \\
\frac{c_{i,j}^{n+1} - c_{i,j}^{n}}{\Delta t} &= K_x \frac{c_{i+1,j}^{n+1/2} - 2c_{i,j}^{n+1/2} + c_{i-1,j}^{n+1/2}}{(\Delta x)^2} \\
&\quad + K_y \frac{c_{i,j+1}^{n+1/2} - 2c_{i,j}^{n+1/2} + c_{i,j-1}^{n+1/2}}{(\Delta y)^2} \\
&\quad - u \frac{c_{i+1,j}^{n+1/2} c_{i-1,j}^{n+1/2}}{2\Delta x}
\end{aligned}
\tag{21}
$$

This method is implicit, since we have used values at the time level $n+1$ for the spatial discretization. In this way, we obtain a system of equations for the set of unknowns $\{c_{i,j}^{n+1}\}$. It turns out that we arrive at the same scheme if the cell averages $\{\bar{c}_{i,j}\}$ are the unknowns (this is a so-called finite volume discretization) and a trapezoidal rule is utilized for the time integration.

5.3. Further numerical details

All of the methods above can be further developed by applying a time-dependent discretization [76]. In practice, one uses a variable grid with finer resolution at locations where the numerical error is high (usually where the concentration gradient is large); this is called adaptive gridding. There are two groups of adaptive gridding techniques called h-refinement ("refine grid locally" and where h stands for the element size) and r-refinement ("relocate a grid").

H-refinement dynamically changes the total number of grid elements within a computational domain for which the original structure remains fixed. This technique is also known as mesh enrichment or local refinement, and it is carried out by subdividing grid elements into smaller self-similar components [16, 77–80]. An example of h-refinement is shown in Figure 6. Higher refinement levels can be achieved by further subdivision of cells.

R-refinement techniques, commonly referred to as mesh moving or global refinement, relocate mesh nodes to regions warranting increased resolution, and subsequently increase grid element concentration in areas where the greatest inaccuracies occur [81, 82]. In this technique, the total number of grid points remains constant. Figure 6 illustrates the conceptual differences of h- and r-refinement. Figure 7 and 8 show these two types of adaptive gridding strategies for simulating the dispersion of air pollutants from a single point source.

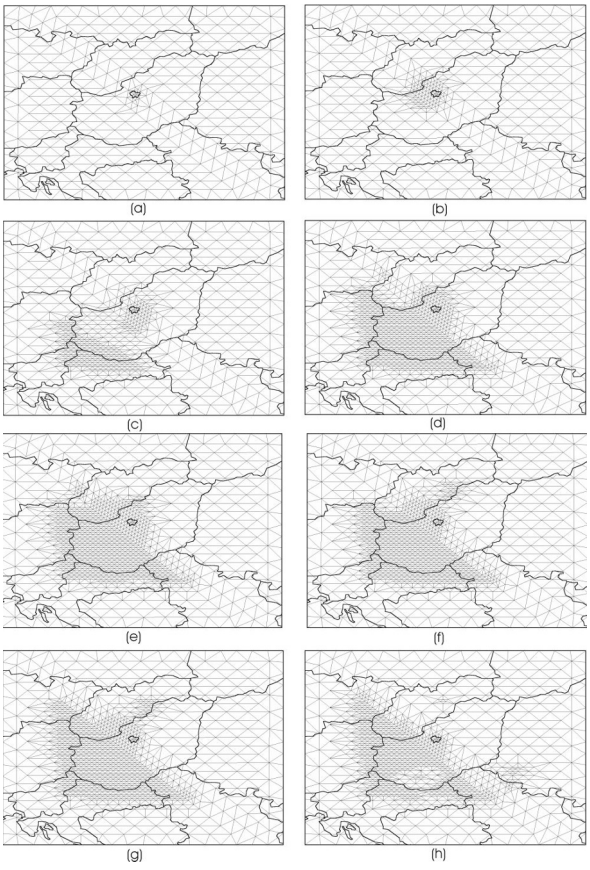

Figure 7. H-refinement applied to simulating photochemical air pollution in Central Europe. The time evolution of the adaptive grid: (a) t_o, (b) t_o + 12 h, (c) t_o + 24 h, (d) t_o + 36 h, (e) t_o + 48 h, (f) t_o + 60 h, (g) t_o + 72 h, (h) t_o + 84 h.

Another generalization is provided by the discontinuous Galerkin method, which differs from the finite element approach in the sense that the basis functions are not necessarily continuous.

In each case, we arrive at a large linear system of sparse matrices to solve, the size of which is the number of unknowns $c_{i,j}$. Typical shape of such matrices is depicted in Figure 9. One has to apply such a solver that can exploit this property. Also, it is especially useful to apply parallel solvers. Several software packages include feasible solvers. The main message of the mathematical analysis is that the discretization parameters cannot be chosen independently.

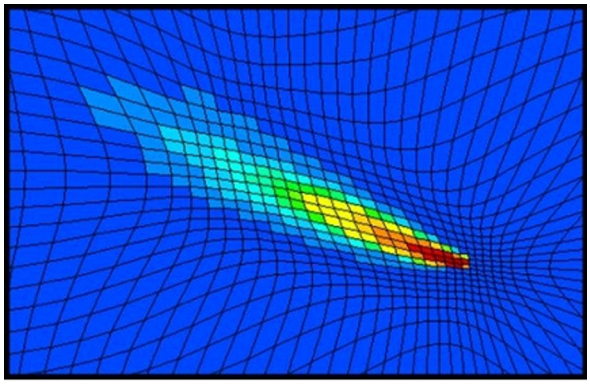

Figure 8. *R*-refinement applied to simulating air pollution dispersion from a point source. Reprinted with permission from [76].

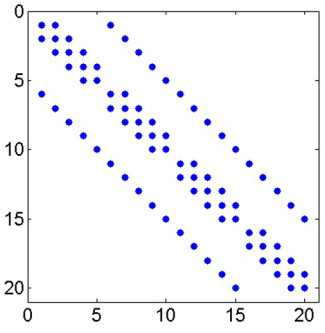

Figure 9. The location of the non-zero elements (thick dots) in the matrix that arises in the time-integration corresponding to the scheme Eq. (21). The number of unknowns is 4×5, the size of the matrix is 20×20, which contains 82 non-zero elements. On the horizontal and the vertical axis show the number of the rows and the columns, respectively.

In practice, for an up-to-date forecast it is favorable to choose a large time step. At the same time, for any explicit method there is a strict constraint for the time step to ensure the convergence of the numerical solution to the real one. In general, if diffusion terms are present then the condition $\Delta t = O\left((\Delta x)^2\right)$ should be satisfied, which – at a precise spatial grid – allows only very tiny time steps. Many of the implicit methods do not require such constraints, but in each time step a large linear system has to be solved. Therefore, one has to evaluate which approach needs less computational resources in every concrete situation.

In practice, we mostly face advection dominated problems, where the average displacement of the pollutant by advection is much more than the displacement caused by diffusion, meaning that $u \gg K_x$ and $v \gg K_y$. The finite element solution of these problems needs special care.

Numerical methods for PDEs have a vast literature. Many of the important principles and methods can be found in general textbooks [83, 84]. The finite difference method is discussed in detail in [85] and a good source on finite volume methods is [86]. A practical exposition of finite element methods can be found in [87], while the application of the discontinuous Galerkin methods for atmospheric problems is discussed in [88].

5.4. Operator splitting

From the mathematical point of view, the basis of air pollution models is a set of partial differential equations that are coupled to each other. The right-hand side of these equations contains several terms describing different physical and chemical sub-processes such as advection, turbulent diffusion, reactions, deposition and emission. The definition of the sub-process is quite flexible, for instance, the advection can be treated as one sub-process, and the horizontal and vertical advection can be interpreted as two separated sub-processes.

The numerical solution of these transport equations is a difficult and challenging computational task, especially in large-scale global models. In these models the number of gridpoints can reach a few hundred thousand, and the number of chemical species can be up to several hundred. Usually these partial differential equations cannot be efficiently solved numerically in one integration step, especially in case of complex reaction mechanisms that take into account the chemical transformation of species at different time scales. This time scale separation of chemical processes causes the stiffness of the system, which means that a stable and convergent numerical solution can be only obtained using a very small time step (i.e., the numerical integration scheme cannot provide solution within a reasonable time). Solving a set of equations that describes all sub-processes at the same time is challenging and, in most cases, impossible. However, the physical background of the sub-processes has been thoroughly investigated, and efficient numerical methods exist for solving the models of these sub-processes (e.g., diffusion and advection equations) as well as to solve the system of stiff equations for chemical reactions. This provides the idea of operator splitting: division of the right-hand side of the original system into several simpler terms and solution of the corresponding systems – which are coupled to each other through the initial conditions – successively in each time step of the numerical solution [89–93]. In this way, the original model is replaced with a model in which the sub-processes take place successively in time. This de-coupling method allows the solution of a few simpler systems instead of the original and more complicated system.

To illustrate the concept of the operator splitting, we present a splitting method used in the Danish Eulerian Model [93–95]. This is a long-range air quality model that has several subsystems describing the horizontal advection

(22), horizontal turbulent diffusion (23), chemical reactions with emissions of air pollutants (24), deposition (25) and vertical turbulent diffusion (26) by the following set of partial differential equations:

$$\frac{\partial c_i^{(1)}}{\partial t} = -\frac{\partial \left(u c_i^{(1)}\right)}{\partial x} - \frac{\partial \left(v c_i^{(1)}\right)}{\partial x}, \tag{22}$$

$$\frac{\partial c_i^{(2)}}{\partial t} = K_x \frac{\partial^2 c_i^{(2)}}{\partial x^2} + K_y \frac{\partial^2 c_i^{(2)}}{\partial y^2}, \tag{23}$$

$$\frac{\partial c_i^{(3)}}{\partial t} = E_i(\vec{x}) + R_i\left(\vec{x}, c_1^{(3)}, c_2^{(3)}, \ldots, c_m^{(3)}\right), \tag{24}$$

$$\frac{\partial c_i^{(4)}}{\partial t} = -k_{\mathrm{dry}} c_i^{(4)} - k_{\mathrm{wet}} c_i^{(4)}, \tag{25}$$

$$\frac{\partial c_i^{(5)}}{\partial t} = -\frac{\partial \left(w c_i^{(5)}\right)}{\partial z} + K_z \frac{\partial^2 c_{i(5)}}{\partial y^2}, \tag{26}$$

for $i = 1, \ldots, m$, where m is the number of chemical species, E_i and R_i are emission and reaction terms, respectively. The original system of PDEs is split into five simpler sub-systems, which can be solved one after the other in each time step in the following way. We assume that the concentration vector $(c_1, \ldots, c_m)$ at the beginning of the time step is known. System (22) is solved by using this vector as an initial condition (starting vector). The obtained solution is an initial vector for the next system (23), and so on. The solution of the fifth system is considered as an approximation to the concentration vector at the end of the time step, i.e, the numerical solution of the full system. This procedure has a competitive advantage, because the sub-systems are easier to solve numerically than the original system. In special cases one of the sub-problems can be even solved analytically. However, it should be noted that the operator splitting may cause inaccuracy in the solution, since the original model is replaced by a model in which the sub-processes take place one after the other, and this error is called splitting error [96–98].

6. Parallel computing

6.1. Introduction to parallel computation

The main limitation of all atmospheric dispersion models beyond their theoretical capabilities is the computational effort needed to calculate predictions with them. There is always a trade-off between speed and accuracy, however, both are requirements for reliable decision support. Naturally, the solution to increase computational performance is parallelization.

For numerical applications, such as the dispersion simulation of air pollutants, parallelization is usually considered on the level of processes and threads that run on different processing units (processor cores, machines) and perform different parts of the computation at the same time. Depending on the memory structure, parallel computing systems can be classified as distributed or shared memory systems. The distinction is fundamental in determining the type of computation that best fits these systems, i.e., which atmospheric dispersion model fits which system.

The most distributed and heterogeneous form of parallel computing is called grid computing [99, 100], in which regular standalone computers in numbers ranging from a few dozen up to several thousand are connected by conventional networks or the Internet. There is high communication latency between computers, therefore in general, these systems best fit for computations that do not require any cooperation (sharing data) between different parts.

Clusters are another, large family of parallel computing systems. Clusters are "homogeneous", consisting of identical computing units, called nodes. A node can be either a regular desktop computer [101], or a mere computing board with basic hardware (CPU, RAM, and network interface) [102]. Nodes are connected by a dedicated high-speed network, and data transfer is managed by specialized software frameworks, e.g. MPI [103] or PVM [104]. Although clusters have distributed memory, these frameworks enable applications to see the entire cluster as a shared memory system.

Multicore workstations [105] and the recently developed technology of using graphics processors (GPUs) for general purpose computation (GPGPU, [106]) are examples of shared memory systems. GPU computing has been successfully applied in atmospheric dispersion modeling [107, 111] as well as in closely related fields [112–116]. Depending on the type of computation, the GPU's speedup over a single CPU can be one or two orders of magnitude [117, 118], and accordingly, a single high-end video card can compete with a smaller cluster of computers.

It is important to note, that theoretically the achievable speedup using parallel computation, regardless of the number of parallel processors used, is limited by the ratio of the non-parallel parts of the computation to the entire run time (Amdahl's law [119]), whenever the size of the computation is fixed. However, the size of the computational task is usually scaled up as the parallel performance increases, therefore the speedup tends to increase with increasing number of processes (Gustafson's law [120]). Indeed, in practice, we tend to increase system size or model complexity if increased parallel performance is available, because the time allowed for an atmospheric dispersion prediction is usually fixed, while the demand for accuracy keeps increasing.

6.2. Parallelization of atmospheric dispersion models

The basic question in parallelization of an atmospheric dispersion calculation is how to split the task to smaller parts that fits well to a certain parallel computing system. In certain cases, parallelization is not necessary at all [121]. The simplicity (hence, shortcomings) of Gaussian models are reflected in their small computational needs: Gaussian models only require simple equation evaluations for a prediction, since these models employ analytical approximation formulas. Generally, they do not need parallel computation.

In Lagrangian models, the computational task is the time-integration of SDEs or ODEs describing the motion of particles. Parallelization is based on exploiting the independence of particle trajectories. Any number of trajectories can be computed independently in parallel, and communication is required only to distribute tasks and gather results. Such a computation is called an embarrassingly parallel problem, and fits well to any parallel computing architecture, including grids [122, 123], clusters of any size [124, 125], and GPUs [107–109].

Most commonly, implementations follow the master-slave paradigm. The parallel computation consists of three steps: First, a master thread assigns particles to available computing units (threads), then each slave thread calculates trajectories in parallel, and finally the master collects partial results from each slave and calculates a statistical average to provide the air pollution prediction (see Figure 10). By repeating these steps multiple times, one can reduce statistical errors and increase the precision of the prediction.

In Eulerian models, the task is computing numerical solutions of PDEs. Here the common technique used is domain decomposition, where the discretized spatial domain is divided to subdomains and assigned to different computing units, and time evolution in these subdomains are calculated in parallel. In principle, a functional decomposition is also possible for highly complex models exploiting operator-splitting: each processor can calculate different operators at the same time. However, in this case the entire domain must be shared between processing units after each iteration, leading to prohibitive communication overhead for distributed memory systems.

The main issue in domain decomposition is calculation of discretized spatial derivatives on the boundaries of the domains, because it requires information from neighbouring domains, assigned to different threads. Therefore, data must be shared regularly with neighbours in a well-coordinated fashion, and the time spent with transferring information must be significantly less than the time spent with computation, for high efficiency and scalability. Therefore, grids are not suited well for Eulerian models; low latency clusters [126–130] and shared memory systems such as multi-core workstations and GPUs [110–112, 114, 116] are the best options. For clusters, communication is coordinated by message passing between neighbour nodes; for shared memory systems each thread waits for neighbours to make a local copy of the boundary of the spatial domain before updating it in the next iteration. The procedure is illustrated in Figure 11. Note, that some clusters (e.g., [102]) feature multidimensional connection topologies between neighbour nodes. Following the same topology for splitting the spatial domain of computation greatly enhances communication efficiency and increases the overall simulation performance.

7. Computational Fluid Dynamics models

In urban air pollution problems, source and receptor points are often located within a few hundred meters from each other, surrounded by a very complex geometry. NWP models have far too coarse resolution to represent the wind field within an urban area, thus existing Eulerian and Lagrangian dispersion models cannot be used.

As urban air quality has become more and more important part of environmental and health protection, computational fluid dynamics (CFD) models have been introduced in environmental modeling. CFD tools are flexible, efficient general purpose solvers of the Navier–Stokes equation [2]:

$$\frac{\partial \vec{v}}{\partial t} + (\vec{v}\nabla)\vec{v} = -\frac{1}{\rho}\nabla p - \vec{g} + \nu_T \nabla^2 \vec{v}, \qquad (27)$$

where $\vec{v}$ is the wind field, ρ is the density, p is the pressure, ν_T is the eddy viscosity and $\vec{g}$ is the gravitational acceleration vector. Eq. (27) is very similar to the one solved in NWP models, however, the coordinate system, grid, boundary conditions and physical parameterizations are completely different [59].

Main parts of a CFD model are the mesh generator, the solver and the turbulence model. As CFD models are often used around complex geometry, a fine grid resolution is required to explicitly calculate turbulence up to a very small scale, which results in extremely high computational costs. However, subgrid-scale turbulence still has to be estimated, which in most cases is assumed to be isotropic. Among the various turbulence models for CFD, the k-ε approach has become the most popular for both engineering and atmospheric applications [131]. k-ε turbulence model uses the Reynolds-averaged (RANS) approach, solving time-averaged equations of motion and considering turbulent fluctuations as eddy viscosity and diffusivity terms. In

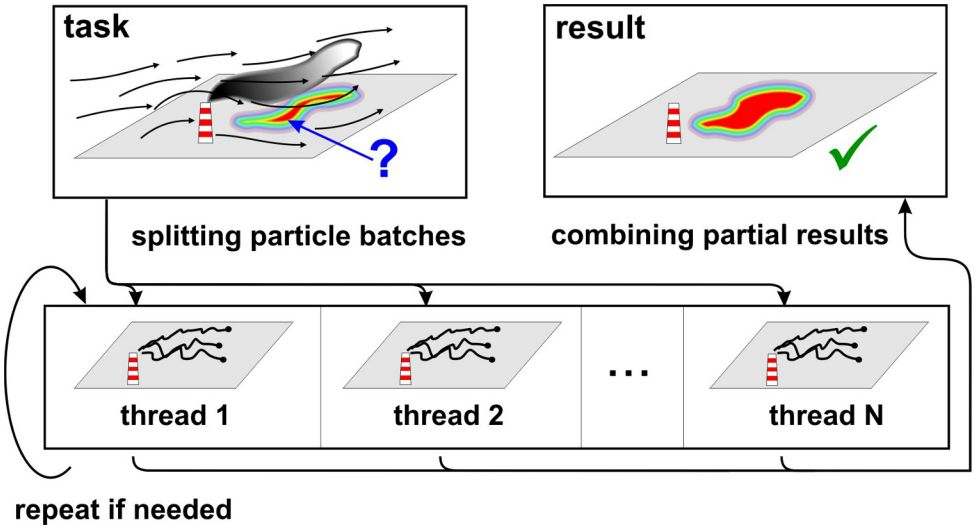

Figure 10. Schematic figure of parallelization in Lagrangian models. Each thread (processors or nodes on clusters and grids, multiprocessors on GPUs) computes trajectories for a batch of particles, and results are then combined to give a complete dispersion prediction.

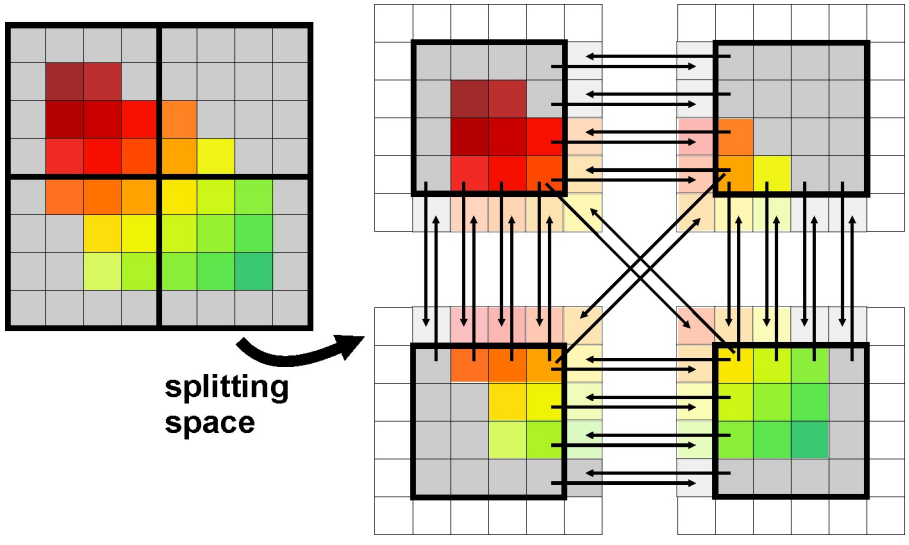

Figure 11. Schematic figure of parallelization in Eulerian models. The simulated space is split between processors (nodes on clusters, multiprocessors on GPUs). In each tile, processors alternate between computing time evolution and transferring updated information to neighbours.

order to estimate these, the k-ε closure introduces two new transport equations for the turbulent kinetic energy and its dissipation rate. However, in the atmosphere, anisotropy of turbulence can cause large errors in k-ε results [132], thus modified atmosphere-oriented turbulence closures are applied [59, 133]. A state-of-the-art solution for turbulence modeling is Large Eddy Simulation (LES), which filters the large scale (anisotropic) and small scale (isotropic) eddies, and performs direct simulation on the former [134]. Despite its huge computational cost, LES has become a popular tool for planetary boundary layer case studies, and its results are often used as a verification dataset for other models [13, 135].

CFD-based street canyon models are widely used to predict air quality in urban and industrial areas [59, 134–139]. However, several weaknesses were pointed out that made CFD results less reliable as the scale increased [132, 133]. Although nesting CFD into NWP models is difficult due to their different coordinates, governing equations and variables, [140] presented promising results using WRF and a three-dimensional CFD code.

Table 4. Recommended approaches for different scales and applications of atmospheric dispersion modeling.

Application	< 1 km	1–10 km	10–100 km	100–1000 km
Online risk management (short runtime is important)	–	Gaussian	Puff	Eulerian
Complex terrain	CFD	Lagrangian	Lagrangian	Eulerian
Reactive materials	CFD	Eulerian	Eulerian	Eulerian
Source-receptor sensitivity	CFD	Lagrangian	Lagrangian	Lagrangian
Long-term average loads	–	Gaussian	Gaussian	Eulerian
Free atmosphere dispersion (volcanoes)	–	Lagrangian	Lagrangian	Lagrangian
Convective boundary layer	(CFD)	Lagrangian	Eulerian	Eulerian
Stable boundary layer	CFD	Lagrangian	Eulerian	Eulerian
Urban areas, street canyon	CFD	CFD	Eulerian	Eulerian

8. Summary

We provided here a brief overview of the problems of air pollution modeling in the atmosphere. We discussed several possible modeling strategies and tools that can be used to support decision makers. The models can be successfully used for different purposes, however, choosing an appropriate model in a particular case is key to handling the problem and successfully estimating the dispersion of air pollutants. Atmospheric dispersion modeling approaches and their applicable scales are summarized in Table 4.

Validation is a necessary step in development in order to test capabilities of models and use models in decision making. There are several opportunities to validate models. For instance, the model performance can be compared to the European Tracer Experiment (ETEX) inventory [141]. ETEX consisted of two releases to atmosphere of tracers (perfluorocarbons) sampled for three days after the beginning of the emission using a sampling network (more than 100 measuring sites) spread over Europe. During these campaigns about 30 modeling research groups could test and analyze the performance and capability their emergency response models. This also contributed to the developments of model parameterizations and showed the importance of the application of high resolution meteorological data. Moreover, validation of the model results can be done against remote sensing data (e.g., sulfur dioxide) or imission data obtained from measuring sites (e.g., ozone, nitrogen oxides).

There are several challenges and possible future developments for air quality modeling. As we discussed earlier NWP and CFD models provide reliable wind data for all scales of atmospheric dispersion simulations, but their connection proved to be difficult. Recent developments of NWPs achieve more and more detailed resolution, CFD models with enhanced computational capacity, parallel computing and LES simulation for anisotropic turbulence are becoming even better for planetary boundary layer simulations. Both the modification of an NWP model to perform microscale simulations (the domain size is ~100 m) [59], and the extension of a CFD software for atmospheric studies hold promise, and these are current topics of research in both the meteorological and environmental engineering fields [132, 134, 140].

Another promising research avenue is in coupling dispersion models to meteorological (or climatological) models [142] and to ensemble forecasting. Ensemble forecasting has been operationally used since 1990's and can incorporate the stochastic nature of weather processes by using either different physical parametrizations or varying initial conditions [143]. Such amodeling approach can reduce the uncertainty in the dispersion pattern of air pollutants.

Finally, we should emphasize that the further development of dispersion models will shift towards multi-scale modeling approaches that can contain sophisticated parameterization of cloud physical processes and biogeochemical interactions.

Acknowledgments

Authors acknowledge the financial support of the Hungarian Research Found (OTKA K77908, K81933, K81975, K104666, K109109, K109361, NK100296 and PD104441), the Zoltán Magyary Postdoctoral Fellowship and the European Union and the European Social Fund (TÁMOP 4.2.4.A-1). F. M. acknowledges partial support by the NSF through Grant No. DEB-0918413.

Appendix: list of acronyms

ADMS	Atmospheric Dispersion Modelling System
AERMOD	American Meteorological Society / Environmental Protection Agency Regulatory Model
ALOHA	Areal Locations of Hazardous Atmospheres
BLP	Buoyant Line and Point Source Dispersion Model
CALINE	California Line Source Dispersion Model
CALPUFF	California Puff Model
CBL	convective boundary layer
CFD	computational fluid dynamics

CMAQ	Community Multi-scale Air Quality Model
CPU	central processing unit
CTDM	Complex Terrain Dispersion Model
CTDMPLUS	Complex Terrain Dispersion Model Plus Algorithms for Unstable Situations
DEM	Danish Eulerian Model
DERMA	Danish Emergency Response Model for the Atmosphere
EPA	Environmental Protection Agency
FLEXPART	Flexible Particle Dispersion Model
GEOS	Goddard Earth Observing System
GIS	geographic information system
GPU	graphics processing unit
GPGPU	general purpose graphics processing unit
HYSPLIT	Hybrid Single-Particle Lagrangian Integrated Trajectory Model
IATA	International Air Transport Association
ISC	Industrial Source Complex Model
LES	large eddy simulation
MPI	multiple protocol interface
NAME	Numerical Atmospheric Dispersion Modelling Environment
NOAA	National Oceanic and Atmospheric Administration
NWP	Numerical Weather Prediction model
OCD	Offshore and Coastal Dispersion model
ODE	ordinary differential equation
PBL	planetary boundary layer
PDE	partial differential equation
PRIME	Plume Rise Model Enhancements
PVM	parallel virtual machine
RAM	random-access memory
RAPTAD	Random Puff Transport and Diffusion
RIMPUFF	Risø Mesoscale Puff Model
RODOS	Realtime Online Decision Support System
SDE	stochastic differential equation
TKE	turbulent kinetic energy
WRF	Weather Research and Forecasting Model

References

[1] Flight disruptions cost airlines $1.7bn, says IATA, BBC News, http://news.bbc.co.uk/2/hi/business/8634147.stm

[2] Stull R. B., An Introduction to Boundary Layer Meteorology. Kluwer Academic Publishers, 1988

[3] Kumar P., Sharan M., Parameterization of the eddy diffusivity in a dispersion model over homogenous terrain in the atmospheric boundary layer, *Atmos. Res.*, 106, 2012, 30–43

[4] Seidel D. J., Ao. C. O., Li K., Estimating climatological planetary boundary layer heights from radiosonde observations: Comparison of methods and uncertainty analysis, *J. Geophys. Res.*, 115, 2010, D16113, doi: 10.1029/2009JD013680

[5] Sriram G., Krishna Mohan N., Gopalasamy V., Sensitivity study of Gaussian dispersion models, *Journal of Scientific and Industrial Research*, 65, 2006, 321–324

[6] Turner D. B., The long lifetime of the dispersion methods of Pasquill in U.S. regulatory air modeling, *J. Appl. Meteorol.*, 36, 1997, 1016–1020

[7] Luna R. E., Church H. W., A Comparison of Turbulence Intensity and Stability Ratio Measurements to Pasquill Stability Classes, *J. Appl. Meteorol.*, 11, 1972, 663–669

[8] Galperin B., Sukoriansky S., Anderson P. S., On the critical Richardson number in stably stratified turbulence, *Atmos. Sci. Lett.*, 8, 2007, 65–69

[9] Cimorelli A. J., Perry S. G., Venkatram A., Weil J. C., Paine R. J., Wilson R. B., Lee R. F., Peters W. D., Brode R. W., AERMOD: A dispersion model for industrial source applications. Part I: General model formulation and boundary layer characterization, *J. Appl. Meteorol.*, 44(5), 2005, 682–693

[10] Perry S. G., CTDMPLUS: A dispersion model for sources near complex topography. Part I: Technical Formulations, *J. Appl. Meteorol.*, 31, 1992, 633–645

[11] Foken T., 50 years of the Monin–Obukhov similarity theory. Bound-Lay. Meteorol., 2006, 119, 431–447

[12] Draxler R. R., Hess G.D., An overview of HYSPLIT_4 modelling system for trajectories, dispersion and deposition, *Aust. Meteorol. Mag.*, 47, 1998, 295–308

[13] Johansson C., Smedman A-S., Högström U., Critical test of the validity of Monin–Obukhov similarity during convective conditions, *J. Atmos. Sci.*, 58, 2001, 1549–1566

[14] Stohl A., Forster C., Frank A., Seibert P., Wotawa, G., Technical note: The Lagrangian particle dispersion model FLEXPART version 6.2, *Atmos. Chem. Phys.*, 5, 2005, 4739–4799

[15] Woodward J. L., Estimating the Flammable Mass of a Vapor Cloud: A CCPS Concept Book Appendix A, doi: 10.1002/9780470935361, 1999

[16] Lagzi I., Kármán D., Turányi T., Tomlin A. S., Haszpra L., Simulation of the dispersion of nuclear contamination using an adaptive Eulerian grid model, *J. Environ. Radioact.*, 75, 2004, 59–82

[17] Mészáros R., Zsély I. G., Szinyei D., Vincze C., Lagzi I., Sensitivity analysis of an ozone deposition model, *Atmos. Environ.*, 43, 2009, 663–672

[18] Mészáros R., Szinyei D., Vincze C., Lagzi I., Turányi T., Haszpra L., Tomlin A.S., Effect of the soil wetness state on the stomatal ozone fluxes over Hungary, *Int. J. Environ. Pollut.*, 36, 2009, 180–194

[19] Sportisse B., A review of parameterizations for modelling dry deposition and scavenging of radionuclides, *Atmos. Environ.*, 41, 2007, 2683–2698

[20] Baklanov A., Sørensen J. H., Parameterisation of radionuclide deposition in atmospheric long-range transport modelling, *Phys. Chem. Earth B.*, 26, 2001, 787–799

[21] Stockie J.M., Mathematics of atmospheric dispersion modelling, *SIAM Rev.*, 53, 2011, 349–372
[22] Namdeo A., Mitchell G., Dixon R., TEMMS: an integrated package for modelling and mapping urban traffic emissions and air quality, *Environ. Model. Softw.*, 17, 2002, 177–188
[23] Sharan, M. and Gopalakrishnan, S. G., Bhopal gas accident: a numerical simulation of the gas dispersion event, *Environ. Model. Softw.*, 12, 1997, 135–141
[24] Li Z., Briggs G. A., Simple PDF models for convectively driven vertical diffusion, *Atmos. Environ.*, 22, 1988, 55–74
[25] Schulman L. L., Strimaitis D. G., Scire J. S., Development and evaluation of the PRIME plume rise and building downwash model, *J. Air Waste Manage. Assoc.*, 50, 2000, 378–390
[26] Abu-Allaban M., Abu-Qudais, H., Impact assessment of ambient air quality by cement industry: a case study in Jordan, Aerosol Air, *Qual. Res.*, 11, 2011, 802–810
[27] Lee S-S., Keener T. C., Dispersion modeling of mercury emissions from coal-fired power plants at Coshocton and Manchester, Ohio. The Ohio J. Sci, 2008, 108, 65–69
[28] Bajwa K. S., Arya S. P., Aneja, V. P., Modeling studies of ammonia dispersion and dry deposition at some hog farms in North Carolina, *J. Air Waste Manage. Assoc.*, 58, 2008, 1198–1207
[29] Krzyzanowski, J., Approaching cumulative effects through air pollution modelling, *Water. Air Soil Pollut.*, 214, 2011, 253–273
[30] Carruthers D. J., Holroyd R. J., Hunt J. C. R., Weng W-S., Robins A. G., Thomson D. J., Smith, F. B., UK-ADMS, a new approach to modelling dispersion in the earth's atmospheric boundary layer, *J. Wind Eng. Ind. Aerod.*, 52, 1994, 139–153
[31] Carruthers D. J., Dyster S. J., McHugh C. A., Factors affecting inter-annual variability of NO_x and NO_2 concentrations from single point sources, *Clean Air and Environmental Protection*, 33, 2003, 15–20
[32] McHugh C. A., Carruthers D. J., Edmunds H. A., ADMS-Urban: an air quality management system for traffic, domestic and industrial pollution, *Int. J. Environ. Pollut.*, 8, 1997, 666–674
[33] Holmes N. S., Morawska L., A review of dispersion modelling and its application to the dispersion of particles: An overview of different dispersion models available, *Atmos. Environ.*, 40, 2006, 5902–5928
[34] Rama Krishna T. V. B. P. S., Reddy M. K., Reddy R. C., Singh R. N., Impact of an industrial complex on the ambient air quality: Case study using a dispersion model, *Atmos. Environ.*, 39(29), 2005, 5395–5407
[35] Silverman, K. C., Tell, J. G., Sargent, E. V. and Qiu, Z., Comparison of the Industrial Source Complex and AERMOD dispersion models: Case study for human health risk assessment, *J. Air Waste Manage. Assoc.*, 57, 2007, 1439–1446
[36] Athanassiadou M., Baker J., Carruthers D., Collins W., Girnary S., Hassell D., Hort M., Johnson C., Johnson K., Jones R., Thomson D., Trought N., Witham C., An assessment of the impact of climate change on air quality at two UK sites, *Atmos. Environ.*, 44, 2010, 1877–1886
[37] Leelőssy Á., Mészáros R., Lagzi I., Short and long term dispersion patterns of radionuclides in the atmosphere around the Fukushima Nuclear Power Plant, *J. Environ. Radioact.*, 102, 2011, 1117–1121
[38] Bubbico R., Mazzarotta, B., Accidental release of toxic chemicals: influence of the main input parameters on consequence calculation, *J. Hazard. Mater.*, 151, 2008, 394–406
[39] Zhang J., Hodgson J., Erkut, E., Using GIS to assess the risks of hazardous materials transport in networks, *Eur. J. Oper. Res.*, 121, 2000, 316–329
[40] Pudykiewicz J., Numerical simulation of the transport of radioactive cloud from the Chernobyl nuclear accident, *Tellus B*, 40B, 1988, 241–259
[41] Piedelievre J. P., Musson-Genon, L., Bompay, F., MEDIA – An Eulerian model of atmospheric dispersion: First validation on the Chernobyl release, *J. Appl. Meteorol.*, 29, 1990, 1205–1220
[42] Dacre H. F., Grant A. L. M., Hogan R. J., Belcher S. E., Thomson D. J., Devenish B. J., Marenco F., Hort M. C., Haywood J. M., Ansmann A., Mattis I., Clarisse L., Evaluating the structure and magnitude of the ash plume during the initial phase of the 2010 Eyjafjallajökull eruption using lidar observations and NAME simulations, *J. Geophys. Res.*, 116, 2011, D00U03, doi: 10.1029/2011JD015608
[43] Mészáros R., Vincze C., Lagzi I., Simulation of accidental release using a coupled transport (TREX) and numerical weather prediction (ALADIN) model, *Időjárás*, 114, 2010, 101–120
[44] Srinivas C. V., Venkatesan R., Baskaran R., Rajagopal V., Venkatraman B., Regional scale atmospheric dispersion simulation of accidental releases of radionuclides from Fukushima Dai-ichi reactor, *Atmos. Environ.*, 61, 2012, 66–84
[45] Brandt J., Mikkelsen T., Thykier-Nielsen S., Zlatev Z., Using a combination of two models in tracer simulations, *Math. Comput. Model.*, 23, 1996, 99–115
[46] Oettl D., Uhmer U., Development and evaluation of GRAL-C dispersion model, a hybrid Eulerian-Lagrangian approach capturing NO-NO_2-O3 chemistry, *Atmos. Environ.*, 45, 2011, 839–847

[47] Pozorski J., Minier J-P., On the Lagrangian turbulent dispersion models based on the Langevin equation, *Int. J. Multiphas. Flow*, 24, 1998, 913–945
[48] Williams M., Yamada T., A microcomputer-based forecasting model: potential applications for emergency response plans and air quality studies., *J. Air Waste Manage. Assoc.*, 40, 1990, 1266–1274
[49] Mikkelsen T., Alexandersen S., Astrup P., Champion H. J., Donaldson A. I., Dunkerley F. N., Gloster J., Sorensen J. H., Thykier-Nielsen S., Investigation of airborne foot-and-mouth disease virus transmission during low-wind conditions in the early phase of the UK 2001 epidemic, *Atmos. Chem. Phys.*, 3, 2003, 2101–2110
[50] Sorensen J. H., Sensitivity of the DERMA long-range Gaussian dispersion model to meteorological input and diffusion parameters, *Atmos. Environ.*, 32, 1998, 4195–4206
[51] Lepicard S., Heling R., Maderich V., POSEIDON/RODOS models for radiological assessment of marine environment after accidental releases: application to coastal areas of the Baltic, Black and North Seas, *J. Environ. Radioact.*, 72, 2004, 153–161
[52] Ghannam K., El-Fadel M., Emissions characterization and regulatory compliance at an industrial complex: An integrated MM5/CALPUFF approach, *Atmos. Environ.*, 69, 2013, 156–169
[53] Levy J. I., Spengler J. D., Hlinka D., Sullivan D., Moon, D., Using CALPUFF to evaluate the impacts of power plant emissions in Illinois: model sensitivity and implications, *Atmos. Environ.*, 36, 2002, 1063–1075
[54] Prueksakorn K., Kim T., Kim S., Kim H., Kim K. Y., Son W., Vongmahadlek C., Review of air dispersion modelling approaches to assess the risk of wind-borne spread of foot-and-mouth disease virus, *J. Environ. Prot.*, 3, 2012, 1260–1267
[55] Zhou Y., Levy J. I., Hammitt J. K., Evans, J. S., Estimating population exposure to power plant emissions using CALPUFF: a case study in Beijing, China, *Atmos. Environ.*, 37, 2003, 815–826
[56] Yamada T., Bunker S., and Moss M., Numerical simulations of atmospheric transport and diffusion over coastal complex terrain, *J. Appl. Meteorol.*, 31, 1992, 565–578
[57] Wang G., Ostoja-Starzewski M., Influence of topography on the Phoenix CO2 dome: a computational study, *Atmos. Sci. Lett.*, 5, 2004, 103–107
[58] Wu J., Lu C-H., Chang S-J., Yang Y-M, Chang B-J., Teng J-H., Three-dimensional dose evaluation system using real-time wind field information for nuclear accidents in Taiwan, *Nucl. Instrum. Methods Phys. Res. A*, 565, 2006, 812–820
[59] Yamada T., Merging CFD and atmospheric modeling capabilities to simulate airflows and dispersion in urban areas, *Comput. Fluid Dyn. J.*, 2004, 13, 329–341
[60] Garner M. G., Hess G. D., Yang, X., An integrated modelling approach to assess the risk of wind-borne spread of foot-and-mouth disease virus from infected premises, *Environ. Model. Assess.*, 11, 2006, 195–207
[61] Long N. Q., Truong Y., Hien P. D., Binh N. T., Sieu L. N., Giap T. V., Phan N. T., Atmospheric radionuclides from the Fukushima Dai-ichi nuclear reactor accident observed in Vietnam, *J. Environ. Radioact.*, 111, 2012, 53–58
[62] McGowan H., Clark A., Identification of dust transport pathways from Lake Eyre, Australia using HYSPLIT, *Atmos. Environ.*, 42, 2008, 6915–6925
[63] Shan W., Yin Y., Lu H., Liang S., A meteorological analysis of ozone episodes using HYSPLIT model and surface data. Atmos. Res., 2009, 93, 767–776
[64] Challa V. S., Indrcanti J., Baham J. M., Patrick C., Rabarison M. K., Young J. H., Hughes R., Swanier S. J., Hardy M. G., Yerramilli A., Sensitivity of atmospheric dispersion simulations by HYSPLIT to the meteorological predictions from a meso-scale model, *Environ. Fluid. Mech.*, 8, 2008, 367–387
[65] Wain A. G., Lee S., Mills G. A., Hess G. D., Cope M. E., Tindale N., Meteorological overview and verification of HYSPLIT and AAQFS dust forecasts for the duststorm of 22–24 October 2002, *Aust. Meteorol. Mag.*, 55, 2006, 35–46
[66] Stohl A., Hittenberger M., Wotawa G., Validation of the Lagrangian particle dispersion model FLEXPART against large-scale tracer experiment data, *Atmos. Environ.*, 32, 1998, 4245–4264
[67] Ryall D. B., Maryon R. H., Validation of the UK Met Office's NAME model against the ETEX dataset, *Atmos. Environ.*, 32, 1998, 4256–4276
[68] de Foy B., Burton S. P., Ferrare R.A., Hostetler C. A., Hair J. W., Wiedinmyer C., Molina, L. T., Aerosol plume transport and transformation in high spectral resolution lidar measurements and WRF-FLEXPART simulations during the MILAGRO Field Campaign, , *Atmos. Chem. Phys.*, 11, 2011, 3543–3563
[69] Warneke C., Froyd K. D., Brioude J., Bahreini R., Brock C. A., Cozic J., de Gouw J. A., Fahey D. W., Ferrare R., Holloway J. S., Middlebrook A. M., Miller L., Montzka S., Schwarz J. P., Sodemann H., Spackman J. R., Stohl, A., An important contribution to springtime Arctic aerosol from biomass burning in Russia, *Geophys. Res. Lett.*, 37, 2010, L01801, doi: 10.1029/2009GL041816
[70] Stohl A., Seibert P., Wotawa G., Arnold D., Burkhart J. F., Eckhardt S., Tapia C., Vargas A., Yasunari T. J.,

Xenon-133 and caesium-137 releases into the atmosphere from the Fukushima Dai-ichi nuclear power plant: determination of source term, atmospheric dispersion, and deposition, *Atmos. Chem. Phys.*, 11, 2011, 28319–28394

[71] Koracin D., Vellore R., Lowenthal D. H., Watson J. G., Koracin J., McCord T., DuBois D. W., Chen L-W. A., Kumar N., Knipping E. M., Wheeler N. J. M., Craig K., Reid S., Regional source identification using Lagrangian stochastic particle dispersion and HYSPLIT backward-trajectory models, , *J. Air Waste Manage. Assoc.*, 61, 2011, 660–672

[72] Povinec P.P., Sykora I., Gera M., Holy K., Brestaková L., Kovácik A., Fukushima-derived radionuclides in ground-level air of Central Europe: a comparison with simulated forward and backward trajectories, *J. Radioanal. Nucl. Ch.*, 295, 2013, 1171–1176

[73] Bey I., Jacob D., Yantosca M., Logan J., Field B., Fiore A., Li Q, Liu H, Mickley L, Schultz M., Global modeling of tropospheric chemistry with assimilated meteorology: Model description and evaluation, *J. Geophys.Res.*, 106, 2001, 23073–23096

[74] Grell G. A., Peckham S. E., McKeen S., Schmitz R., Frost G., Skamarock W. C., Eder B., Fully coupled "online" chemistry within the WRF model, *Atmos. Environ.*, 39, 2005, 6957–6975

[75] Wang K., Zhang Y., Jang C., Phillips S., Wang B., Modeling intercontinental air pollution transport over the trans-Pacific Region in 2001 using Community Multiscale Air Quality modeling system, *J. Geophys. Res.*, 114, 2009, D04307

[76] Garcia-Menendez F., Odman M. T., Adaptive grid use in air quality modeling, *Atmosphere*, 2, 2011, 484–509

[77] Ghorai S., Tomlin A. S., Berzins M., Resolution of pollutant concentrations in the boundary layer using a fully 3D adaptive gridding technique, *Atmos. Environ.*, 34, 2000, 2851–2863

[78] Lagzi I., Tomlin A. S., Turányi T., Haszpra L., Mészáros R., Berzins M., The simulation of photochemical smog episodes in Hungary and Central Europe using adaptive gridding models, *Lect. Notes Comp. Sci.*, 2074, 2001, 67–77

[79] Lagzi I., Tomlin S. A., Turányi T., Haszpra, L., Modelling photochemical air pollutant formation in Hungary using an adaptive grid technique, *Int. J. Environ. Pollut.*, 36, 2009, 44–58

[80] Tomlin A. S., Ghorai S., Hart G., Berzins M., 3-D Multi-scale air pollution modelling using adaptive unstructured meshes, *Environ. Model. Softw.*, 15, 2000, 681–692

[81] Zegeling P. A., R-refinement with finite elements or finite differences for evolutionary PDE models, *Appl. Numer. Math.*, 26, 1998, 97–104

[82] Zegeling P. A., Lagzi I., Izsak F., Transition of Liesegang precipitation systems: simulations with an adaptive grid PDE method, *Commun. Comput. Phys.*, 10, 2011, 867–881

[83] Ascher U., Numerical methods for evolutionary differential equations. Computational science and engineering. Society for Industrial and Applied Mathematics (SIAM), Philadelphia, 2008

[84] Grossmann C., Roos H., Stynes M., Numerical Treatment of Partial Differential Equations. Universitext, Springer, Berlin, 2007

[85] Thomas J. W., Numerical partial differential equations: finite difference methods, volume 22 of Texts in Applied Mathematics. Springer-Verlag, New York, 1995

[86] Versteeg H., Malalasekera W., An introduction to computational fluid dynamics: the finite volume method. Pearson Education Australia, 2007

[87] Huebner K., The Finite Element Method for Engineers. A Wiley-Interscience publication. Wiley, New York, 2001

[88] Nair R. D., Thomas S. J., Loft R. D., A discontinuous Galerkin transport scheme on the cubed sphere. Mon. Weather Rev., 2005, 133, 814–828

[89] Faragó I., Havasi Á., Operator splitting and their applications, Mathematics Research Development Series, Nova Science Publishers, Inc., New York, 2009

[90] Lanser D., Verwer J. G., Analysis of operator splitting for advection-diffusion-reaction problems in air pollution modelling, *J. Compute. Appl. Math.*, 111, 1999,201–216

[91] Marchuk G. I., Methods of Splitting. Nauka, Moscow, 1988 (in Russian)

[92] Yanenko N. N., On convergence of the splitting method for heat equation with variable coefficients. Journal of Computational Mathematics and Mathematical Physics 2, 1962 (in Russian)

[93] Zlatev Z., Computer Treatment of Large Air Pollution Models, Kluwer Academic Publisher, 1995

[94] Dimov I., Faragó I., Havasi Á., Zlatev Z., Operator splitting and commutativity analysis in the Danish Eulerian Model, *Math. Comput. Simul*, 67, 2003, 217–233

[95] Dimov I., Faragó I., Havasi Á., Zlatev, Z., Different splitting techniques with application to air pollution models, *Int. J. Environ. Pollut.*, 32(2), 2008, 174–199

[96] Strang G., On the construction and comparison of difference schemes, *SIAM J. Numer. Anal.*, 5, 1968, 506–517

[97] Csomós P., Havasi Á., Faragó I., Weighted sequential splittings and their analysis, *Comp. Math. Appl.*, 50,

2005, 1017–1031
[98] Strang G., Accurate partial difference methods I: Linear Cauchy problems, *Arch. Ration. Mech. An.*, 12, 1963, 392–402
[99] Foster I., Kesselman C., Tuecke S., The anatomy of the grid, *Intl. J. High Perf. Comput. Appl*, 15, 2001, 200–222
[100] Jacob B., Brown M., Fukui K., Trivedi N., Introduction to Grid computing. IBM Redbooks, Vervante, Springville, Utah, 2005
[101] Sterling T. L, Bell G., Beowulf Cluster Computing With Linux, MIT Press, 2002
[102] Adiga N. R., Blumrich M. A., Chen D., Coteus P., Gara A., Giampapa M. E., Heidelberger P., Singh S., Steinmacher-Burow B. D., Takken T., Tsao M., Vranas P., Blue Gene/L torus interconnection network, *IBM J. Res. Dev.*, 49, 2005, 265–276
[103] Hempel R., The MPI standard for message passing. Proc. Intl. Conf. and Exhibit. On High Perf. Comp and Networking II, 1994, 247–252
[104] Sunderam V. S., PVM: A framework for parallel distributed computing, *Concurrency-Pract. Ex.*, 2, 1990, 315–339
[105] Sun X.-H., Chen Y., Reevaluating Amdahl's law in the multicore era, *J. Parallel Distrib. Comput.*, 70, 2010, 183–188
[106] General Purpose Computation on Graphics Hardware, http://gpgpu.org/
[107] Mészáros R., Molnár F., Izsák F., Kovács T., Dombovári P., Steierlein Á., Nagy R., Lagzi I., Environmental modeling using graphical processing unit with CUDA, *Időjárás*, 116, 2012, 237–251
[108] Molnár F., Szakály T., Mészáros R., Lagzi I., Air pollution modelling using a Graphics Processing Unit with CUDA, *Comput. Phys. Commun.*, 181, 2010, 105–112
[109] Pardyjak E. R., Singh B., Norgren A., Willemsen P., Using video gaming technology to achieve low-cost speed up of emergency response urban dispersion simulations, in: Seventh Symposium on the Urban Environment, University of Utah, Salt Lake City and University of Minnesota, Duluth, 2007
[110] Senocak I., Thibault J., Caylor M., Rapid-response urban CFD simulations using a GPU computing paradigm on desktop supercomputers, in: Eighth Symposium on the Urban Environment, Phoenix, Arizona, 2009, J19.2
[111] Simek V., Dvorak R., Zboril F., Kunovsky J., Towards accelerated computation of atmospheric equations using CUDA, in: Proceedings of the UK Sim 2009. 11th International Conference on Computer Modelling and Simulation, 2009, 449–454
[112] Januszewski M., Kostur M., Accelerating numerical solution of stochastic differential equations with CUDA, *Comput. Phys. Commun.*, 181, 2010, 183–188
[113] Michéa D., Komatitsch D., Accelerating a three-dimensional finite-difference wave propagation code using GPU graphics cards, *Geophys. J. Int.*, 182, 2010, 389–402
[114] Micikevicius P., 3D Finite difference computation on GPUs using CUDA. Proc. 2nd Workshop General Purpose Processing on Graphics Processing Units, ACM, 2009, 79–84
[115] Molnár F., Izsák F., Mészáros R., Lagzi I., Simulation of reaction-diffusion processes in three dimensions using CUDA, *Chemometr. Intell. Lab.*, 108, 2011, 76–85
[116] Sanderson A. R., Meyer M. D., Kirby R. M., Johnson C. R., A framework for exploring numerical solutions of advection–reaction–diffusion equations using a GPU-based approach, *Comput. Vis. Sci.*, 12, 2009, 155–170
[117] Che S., Boyer M., Meng J., Tarjan D., Sheaffer J. W., Skadron K., A performance study of general purpose applications on graphics processors using CUDA. J. Parallel Distr. Com., 2008, 68, 1370–1380
[118] Garland M., Le Grand S., Nickolls J., Anderson J., Hardwick J., Morton S., Phillips E., Zhang Y., Volkov, V., Parallel computing experiences with CUDA, *Micro IEEE*, 28, 2008, 13–27
[119] Krishnaprasad S., Uses and abuses of Amdahl's law, *J. Comp. Sci. Coll.*, 17, 2001, 288–293
[120] Gustafson J., Re-evaluating Amdahl's law, *Communications of the ACM*, 31, 1988, 532–533
[121] El-Nashar A. I., To Parallelize or not to parallelize, speed up issue, *Int. J Dist. Parallel Syst.*, 2, 2011, 2
[122] Ostromsky T., Zlatev Z., Parallel and GRID implementation of a large scale air pollution model. Numerical Methods and Applications Lect., *Notes Comput. Sc.*, 4310, 2007, 475–482
[123] Todorova A., Syrakov D., Gadjhev G., Georgiev G., Ganev K.G., Prodanova M., Miloshev N., Spiridonov V., Bogatchev A., Slavov K., Grid computing for atmospheric composition studies in Bulgaria, *Earth Sci. Inf.*, 3, 2010, 259–282
[124] Roberti D. R., Souto R, P., de Campos Velho H. F., Degrazia G. A., Anfossi D., Parallel implementation of a Lagrangian stochastic model for pollutant dispersion, *Int. J. Parallel Program.*, 33, 2005, 485–498
[125] Srinivas C. V., Venkatesan R., Muralidharan N. V., Das S., Dass H., Kumar P.E., Operational mesoscale atmospheric dispersion prediction using a parallel computing cluster, *J. Earth Syst. Sci.*, 115, 2006, 315–332
[126] Alexandrov V. N., Owczarz W., Thomson P. G., Zlatev

Z., Parallel runs of a large air pollution model on a grid of Sun computers, *Math. Comput. Simul.*, 65, 2004, 557–577

[127] Georgiev K., An algorithm for parallel implementations of an Eulerian smog model. Numerical Methods and Applications Lect., *Notes Comput. Sc.*, 2542, 2003, 463–470

[128] Georgiev K., Ostromsky T., Zahari Z., New parallel implementation of an air pollution computer model – performance study on an IBM blue gene/p computer. Large-Scale Scientific Computing Lect. *Notes Comput. Sc.*, 7116, 2012, 283–290

[129] Ostromsky T., Zlatev Z., Parallel implementation of a large-scale 3-D air pollution model. Large-Scale Scientific Computing Lect, *Notes Comput. Sc.*, 2179, 2001, 309–316

[130] Philippe C., Coppalle A., Atmospheric dispersion and chemical pollutant transformation simulated with parallel calculations using two PC clusters, *Int. J. Environ. Pollut.*, 22, 2004, 133–143

[131] Chen Q., Prediction of room air motion by Reynolds-stress models. Build. Environ., 1996, 31(3), 233–244

[132] Rossi R., Iaccarino G., Numerical simulation of scalar dispersion downstream of a square obstacle using gradient-transport type models, *Atmos. Environ.*, 43, 2009, 2518–2531

[133] Baklanov A., Application of CFD methods for modelling in air pollution problems: possibilities and gaps, *Environ. Monit. Assess.*, 65, 2000, 181–189

[134] Cheng W. C., Liu, C-H., Large-eddy simulation of flow and pollutant transports in and above two-dimensional idealized street canyons, *Bound-Lay. Meteorol.*, 139, 2011, 411–437

[135] Li X-X., Liu C-H., Leung D. Y. C., Large-eddy simulation of flow and pollutant dispersion in high-aspect-ratio urban street canyons with wall model, *Bound-Lay. Meteorol.*, 129, 2008, 249–268

[136] Balczó M., Balogh M., Goricsán I., Nagel T., Suda J. M., Lajos T., Air quality around motorway tunnels in complex terrain: computational fluid dynamics modeling and comparison to wind tunnel data, *Időjárás*, 115, 2011, 179–204

[137] Di Sabatino S., Buccolieri R., Pulvirenti B., Britter R. E., Flow and pollutant dispersion in street canyons using FLUENT and ADMS-Urban. *Environ. Model. Assess.*, 13, 2008, 369–381

[138] Milliez M., Carissimo B., Numerical simulations of pollutant dispersion in an idealized urban area, for different meteorological conditions, *Bound-Lay. Meteorol.*, 122(2), 2007, 321–342

[139] Tominaga Y., Mochida A., Yoshie R., Kataoka H., Nozu T., Yoshikawa M., Shirasawa, T., AIJ guidelines for practical applications of CFD to pedestrian wind environment around buildings, *J. Wind Eng. Ind. Aerod.*, 96, 2008, 1749–1761

[140] Tewari M., Kusaka H., Chen F., Coirier W.J., Kim S., Wyszogrodzki A. A., Warner, T. T., Impact of coupling a microscale computational fluid dynamics model with a mesoscale model on urban scale contaminant transport and dispersion, *Atmos. Res.*, 96, 2010, 656–664

[141] Van Dop, H., Addis, R., Fraser, G., Girardi, F., Graziani, G., Inoue, Y., Kelly, N., Klug, W., Kulmala, A., Nodop, K., Pretel, J., ETEX: A Europian Tracer Experiment; Observations, dispersion modelling and emergency response, *Atmos. Environ.* 32, 1998, 4089–4094

[142] Zhang, Y: Online-coupled meteorology and chemistry models: history, current status, and outlook, *Atmos. Chem. Phys.*, 8, 2008, 2895–2932

[143] Molteni, F.; Buizza, R.; Palmer, T. N.; Petroliagis, T., The ECMWF Ensemble Prediction System: Methodology and validation,*Q. J. Roy, Meteor. Soc.*, 122, 1996, 73–119